Mass transfer of an impinging jet confined between parallel plates

by O. A. Moreno R. H. Katyl J. D. Jones P. A. Moschak

An understanding of the mass transfer behavior of an impinging jet can be usefully applied to wet chemical processes such as water rinsing, photoresist development, and metal etching or plating. Theoretical and experimental methods were used to study the mass transfer characteristics of an axisymmetric impinging jet confined between two parallel plates. Such a configuration was used because of its potential applicability to the fabrication of printed wiring boards. The CFD (computational fluid dynamics) method was used to model fluid flow and mass transfer. An electrochemical probe based on the ferro-ferricyanide system was used to experimentally determine the mass transfer coefficients and to evaluate the applicability of the theoretical methods used. An etching method was used to characterize the mass transfer rates in a typical cupric chloride etching solution. A new observation of the effect of jet instability on the etching rate in the central impingement zone is discussed.

Introduction

In the fabrication of printed wiring boards (PWBs), exposure to process chemicals takes place by either immersion in tanks or conveyance through spray chambers. Both of these approaches have met with difficulties with regard to uniformity across the PWB surface. The use of arrays of impinging jets is an alternative method which may improve uniformity.

Arrays of impinging jets have been applied to chemical processing in electronic packaging by Bard et al. [1]. Applicability to jet electroplating has been discussed by Pellegrino [2], and mass transfer studies have been carried out by Chin and Tsang [3], and by Alkire and Chen [4]. A related area involving the application of toner in copier machines has been discussed by Zin [5]. A recent study of water evaporation with single and multiple impinging air jets was reported by Trabold and Obot [6]; their paper included relevant references.

In the related area of heat transfer, impinging gas jets are used, for example, for cooling in glass manufacture [7–9], for heating and drying in the paper industry [10], and for cooling within jet engine turbines. Martin [11] has summarized the heat transfer work in this area. Recent

[•]Copyright 1993 by International Business Machines Corporation. Copying in printed form for private use is permitted without payment of royalty provided that (1) each reproduction is done without alteration and (2) the Journal reference and IBM copyright notice are included on the first page. The title and abstract, but no other portions, of this paper may be copied or distributed royalty free without further permission by computer-based and other information-service systems. Permission to republish any other portion of this paper must be obtained from the Editor.

studies of heat transfer under a single impinging jet have been carried out by Liu et al. [12], Stevens and Webb [13], and Al-Sanea [14].

As a simple example of a manufacturing process for which improvements should be achievable through the use of impinging jets, let us consider a rinsing operation. When the rinsing involves dissolved species, the process is limited by mass transfer. Increasing the mass transfer rate of a rinsing device should save space, facilitating the use of multiple counter-current stages and thus reducing the amount of water required while leading to more effective cleaning of the product surface. This should reduce operating costs and, in some cases, the volume of hazardous waste. Other related but more complex processes for which the use of impinging jets may be advantageous include metal etching, photoresist development, surface preparation, and coating.

The fluid dynamics and mass transfer characteristics of a rinsing device can be optimized by choosing an appropriate jet configuration. For highly volatile solvent-based processes, the intent would be to perform the same function as a spray device while significantly reducing environmental emission due to atomization of the processing fluid. For chemical reactions that are transport-limited, the intent would be to increase the rate of reaction or to improve uniformity, the first of which should reduce processing time while increasing throughput or decreasing equipment size, and the second of which should increase product quality.

Because of the complexity of the phenomena occurring under an impinging jet, certain approximations must be made in discerning its behavior. Perfect mathematical models cannot be afforded to describe these processes. Therefore, our approach has relied on process insight provided by a simplified mathematical model, knowledge of a successful technique used extensively in electrochemical engineering research to measure mass transfer coefficients, and a bit of intuition involving the practice of metal etching to gain a better understanding of this wet processing technique used extensively in the fabrication of PWBs.

This paper pertains to methods we have used to characterize the fluid dynamics and mass transfer properties of a basic building block of jet array processing devices: a single impinging jet confined between parallel plates. The configuration was chosen because of its potential application as a processing device in the fabrication of PWBs. The approach used was a simplified example of a cost-effective strategy to obtain process information for engineering design purposes. The next part of this paper describes the fluid motion studied, followed by discussions of the experimental and theoretical methods used and associated results obtained.

• Description of fluid motion

An impinging jet is useful for obtaining high rates of heat or mass transfer. Much of this increase occurs locally near the point where the fast-moving jet collides with the working surface. **Figure 1** shows the geometry of a typical impinging jet discharging into a confinement of two parallel plates. The gap separating the plates is H. The several regions of interest have been discussed in the literature [3, 4, 11]; these are the following: the jet region, the impingement zone I, the wall jet region W, the transition region T, and the established flow region E.

For electrochemical reactions at the surface beneath the jet, the transport of ions of species, i, into or out of the surface is described by a flux, N_i , in units of (moles)/(area-time). The flux of ions is related to the bulk and surface ion concentrations by the mass transport law,

$$N_{i} = k [C_{i}(surface) - C_{i}(bulk)], \tag{1}$$

where k is the mass transfer coefficient in units of velocity; it is an overall measure of the transfer rate and includes the effects of fluid motion.

In our discussion, we make use of correlations obtained from dimensional analysis [15]. The parameters for describing the mass transfer properties of the system are the Reynolds number Re, the Sherwood number Sh, and the Schmidt number Sc. The characteristic dimension used for these parameters is the diameter of the nozzle. Re is a measure of the ratio of inertial to viscous effects; Sh is the ratio of mass to molecular diffusivities; and Sc is the ratio of momentum to molecular diffusivities. For a special case described later, Re and Sh are defined using the radial distance r from the nozzle axis as the characteristic dimension. The defining equations are

$$Re_{\rm d} = \frac{V_{\rm N} d_{\rm N}}{\nu}, Re_{\rm r} = \frac{V_{\rm N} r}{\nu},$$

$$Sh_{\rm d} = \frac{kd_{\rm N}}{D_{\rm i}}$$
, $Sh_{\rm r} = \frac{kr}{D_{\rm i}}$, and $Sc = \frac{\nu}{D_{\rm i}}$, (2)

where ν is the kinematic viscosity of the fluid, $D_{\rm i}$ is the diffusion coefficient for the ion of interest, $d_{\rm N}$ is the diameter of the nozzle, and $V_{\rm N}$ is the average fluid velocity in the nozzle of the jet. The parameters $Sh_{\rm d}$ and $Re_{\rm d}$ are used to describe effects in the impingement zone, while $Sh_{\rm r}$ and $Re_{\rm r}$ are used to describe effects in areas at a radial distance r away from the impingement point.

• Electrochemical probe method

A precise means of determining mass transfer rates is through the monitoring of local currents in the controlled electrolysis of a ferricyanide ion in the presence of sodium hydroxide in aqueous solution. In the following description, the cation, or ferricyanide ion, undergoes reduction at the cathode, while the anion, or ferrocyanide

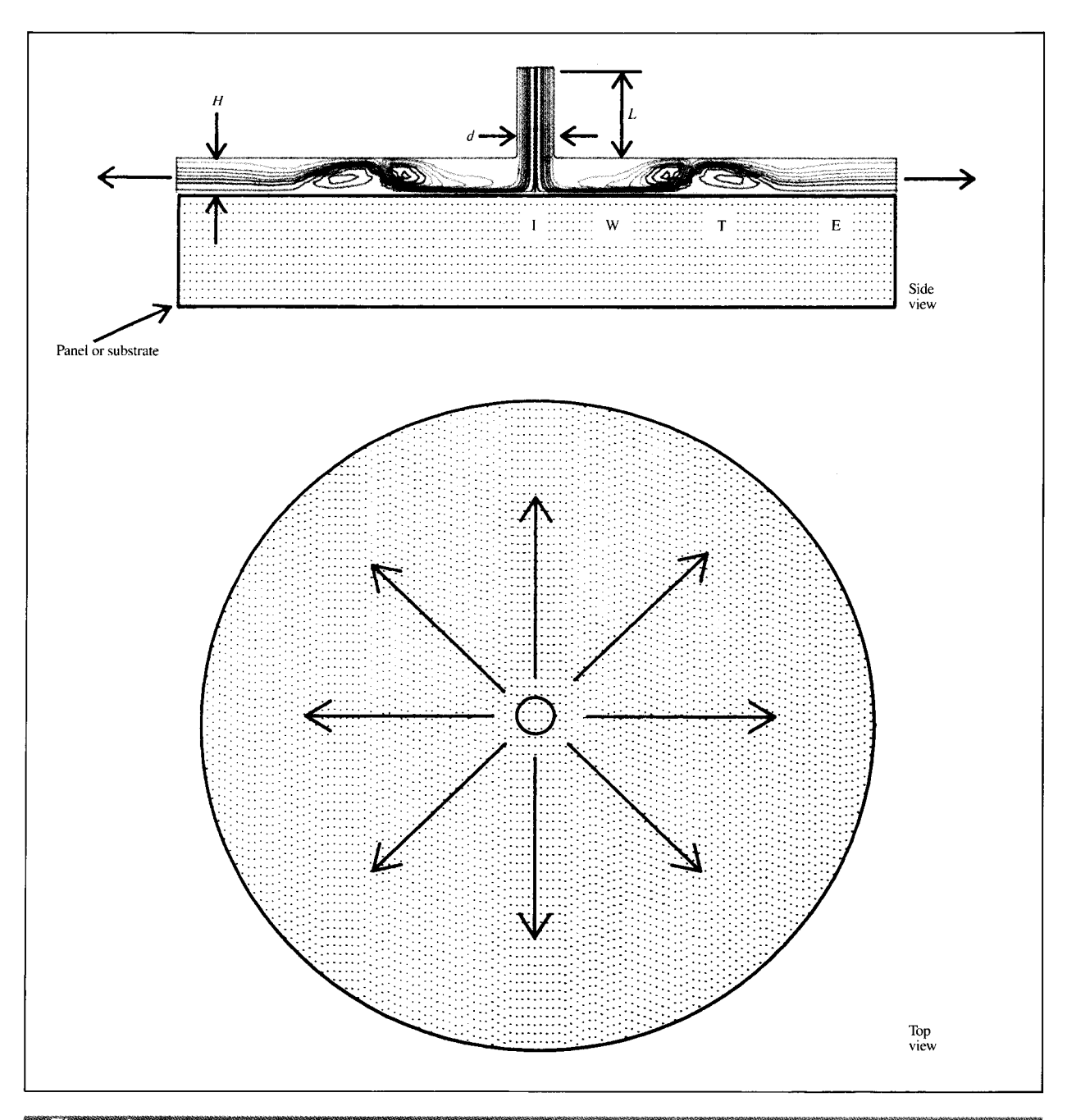


Figure 1

Configuration of a typical impinging jet. The liquid exits the jet orifice in a well-defined column, travels a short distance, and strikes the surface. Flow direction is indicated by arrows. I = impingement zone, W = wall jet region, T = transition zone, E = established flow region. The gap between the plates is H. The boundary layer near the impingement point is relatively small, enhancing mass transfer. The colored lines represent different streamlines.

ion, undergoes oxidation at the anode.* As described by Reiss and Hanratty [16, 17] and by Mizushina [18], this

*We use the cation terminology for the ferricyanide ion, although it has a negative charge.

technique uses a microelectrode (or probe) embedded in the surface of an insulator to determine the rates of mass transfer with an electrical current produced by a driving voltage. A cross section of a typical electrochemical cell

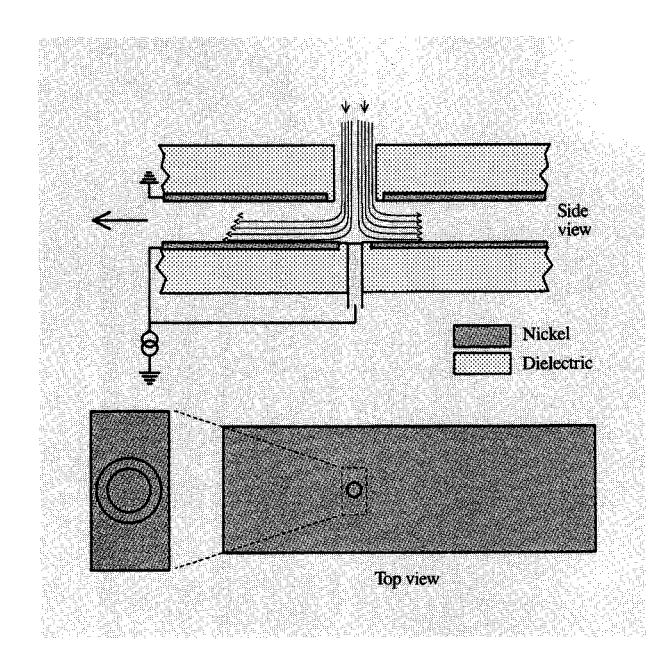


Figure 2

Typical electrochemical cell used to determine mass transfer rates. Probe was located directly beneath the jet.

used to determine mass transfer rates is shown in **Figure 2**. The following reactions occur at the cathode and anode electrodes:

$$Fe(CN)_6^{3-} + e^- \rightleftharpoons Fe(CN)_6^{4-}$$
. (3)

These reactions occur on surfaces of pure nickel which are held at a differential voltage of 0.85 V. As the applied voltage is increased from zero, the current increases and levels off at a limiting current value, where the reaction rate is limited by the rate of diffusion to the electrode surface, and not by the rate of the chemical reaction. This has been shown to be a good assumption for the widely used ferro-ferricyanide system. Also, the cell must be designed so that transport at the electrode of interest, the cathode, limits the reaction. This is achieved by making the opposite electrode, the anode, of much larger area.

For the electrochemical system, the mass-transferlimiting current can be related to the Sherwood number according to the following relationships [19], which can be developed from the mass transfer law in (1), by assuming that n electrons are transferred in the reactions

$$Sh_{\rm d} = \frac{s_{\rm i}d_{\rm N}I}{D_{\rm i}\Delta C_{\rm i}nAF} \tag{4}$$

and

$$Sh_{\rm r} = \frac{s_{\rm r}rI}{D_{\rm r}\Delta C_{\rm r}nAF}.$$
 (5)

In these equations, s_i is the stoichiometric coefficient of the collected ion species, i, in the microelectrode reaction of Equation (3), d_N is the diameter of the nozzle in meters, r is the radial distance from the nozzle axis, I is the electrical current through the electrode of interest in amperes, D_i is the diffusion coefficient of species i in m^2/s , ΔC_i is the difference in concentration of species i between the bulk of the solution and the surface of the microelectrode, A is the area of each microelectrode in m^2 , and F is the Faraday constant. If the measurements are made at the mass-transfer-limiting current, the concentration at the surface is essentially zero, and the concentration term ΔC_i reduces to the bulk concentration value.

The dependence of mass transfer on the fluid properties is expected to follow the well-known Chilton-Colburn analogy established between heat transfer and mass transfer coefficients [20–22]:

$$Sh = ARe^b Sc^{1/3}. (6)$$

The values found for the coefficients A and b in this work are discussed in a subsequent section. The exponent of the Schmidt number is close to 1/3 for many electrochemical situations. A theoretical treatment in [3] gives an asymptotic form for the deviations from $Sc^{1/3}$. For the large Sc values of the electrolytes of this work, the correction is less than 1%.

• Controlled etching method

A method used in PWB fabrication to obtain copper circuit lines is metal etching. In this process, a concentrated aqueous solution of cupric chloride is used to etch the copper metal that is covered with a resist mask. The etching solution is acidified with hydrochloric acid to improve the etching rate and speed up the process.

In simplified terms, the chloride ions in the etching solution interact with the copper metal according to the reaction

$$Cu^{0} + 3Cl^{-} \rightarrow CuCl_{3}^{-2} + e^{-}.$$
 (7)

The CuCl₃⁻² product is transported from the surface through the diffusion layer to the bulk. Georgiadou [23] has conducted experimental and theoretical studies of copper etching with solutions of cupric chloride and hydrochloric acid. By using a rotating disk electrode, it was observed that copper dissolves with a Tafel-like active region at low overpotentials. The dissolution current reached a maximum peak followed by a sharp drop to a minimum. At higher potentials the current rose to a plateau that was influenced by the rotation speed, as in a mass-transfer-limited process. In this region, the rate-limiting step is the transport of chloro-complexes of Cu⁺ from a CuCl_(s)-saturated surface. From these observations and other experimental evidence in [23], it was determined that etching of copper with an acidic cupric chloride

solution could be approximated as a mass-transfer-limited process.

In a typical etching situation, Sherwood numbers can be calculated from the etch rate E from simple mass balance considerations, namely

$$Sh_{\rm d} = \frac{\rho_{\rm Cu} d_{\rm N} E}{D_{\rm (CuCl_3^{-2})} \Delta C_{\rm (CuCl_3^{-2})} MW_{\rm Cu\ metal}}$$
(8)

and

$$Sh_{\rm r} = \frac{\rho_{\rm Cu} rE}{D_{\rm (CuCl_3^{-2})} \Delta C_{\rm (CuCl_3^{-2})} MW_{\rm Cu\ metal}},$$
 (9)

where ρ_{Cu} is the density of copper metal, d_{N} is the nozzle diameter, E is the etch rate in meters per second (m/s), $D_{(\mathrm{CuCl_3}^{-2})}$ is the diffusion coefficient of aqueous $\mathrm{CuCl_3}^{-2}$ in m^2/s , $\Delta C_{(\mathrm{CuCl_3}^{-2})}$ is the difference in concentration between the surface (assumed to be saturated $\mathrm{CuCl_3}^{-2}$) and the bulk of the solution, and $MW_{\mathrm{Cu}\ \mathrm{metal}}$ is the molecular weight of copper.

• Fluid equations and formulation of the CFD model
The fluid motion illustrated in the present work was
computed numerically by a commercial finite element
program, FIDAP™ [24]. The flow simulated was that of a
single impinging jet of circular cross section, as in the
electrochemical and controlled etching systems used in this
study. The concentration distribution of the cation in the
electrochemical probe system was simulated using the
one-electron model of Equation (3). For simplicity of
calculation, only flows with Reynolds numbers below 1800
were analyzed. Most real flows are turbulent in nature and
have additional complexities.

The equations considered in the finite element method were the Navier-Stokes equations for the fluid flow and the chemical mass transport equations for a flowing fluid [25]. Several assumptions simplified the analysis of this problem. The electrochemical cell was assumed to be isothermal, so solution of the energy balance equation was not required. Also, because the aqueous solution is incompressible, density was assumed to be constant; in addition, gravitational effects were ignored. The chemical species are nonreactive in the bulk of the solution, so their transport equations were assumed to be uncoupled. Their motion was assumed to be governed by both Fick's law of diffusion and also convection by the solution. A large background concentration of Na and OH ions existed, serving to minimize ohmic potential drops and ion migration due to electric field effects. Thus, the bulk concentrations of the diffusing species were assumed to be independent of one another and to be relatively unaffected by the applied potential field.

In the equations that were thus obtained, conservation of mass is stated mathematically with the continuity

equation. Under the assumption of incompressibility, the density ρ is constant, giving simply

$$\nabla \cdot \mathbf{u} = 0. \tag{10}$$

Transport of momentum by the fluid is described by the momentum equation

$$\rho \frac{\partial \mathbf{u}}{\partial t} + \rho \mathbf{u} \cdot \nabla \mathbf{u} = -\nabla p + \mu \nabla^2 \mathbf{u}. \tag{11}$$

The successive terms in the equations describe the balance of inertia, convection, pressure drop, and viscous effects at a point in the fluid. Equation (11) is valid for nonsteady flow situations; for steady flow the time derivative in the first term vanishes. Motion of ions of chemical species, i, is given by a transport equation for each ion:

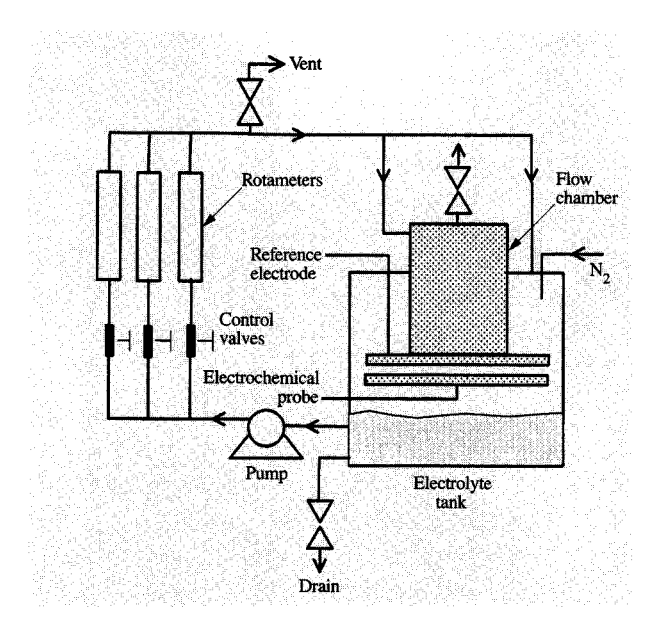
$$\frac{\partial C_i}{\partial t} + \mathbf{u} \cdot \nabla C_i - D_i \nabla^2 C_i = 0. \tag{12}$$

In the above equations, \mathbf{u} , p, and ρ are the fluid velocity, pressure, and density, respectively; C_i is the chemical concentration of species i, and D_i is the diffusion coefficient of the ion.

The boundary condition to be applied to the flow is the no-slip condition, which requires that the velocity component tangential to any surface be zero. Across outlet surfaces the velocity components are not specified, and are computed using the finite element solution procedure. The axial component of velocity at the inlet to the nozzle was assumed to have a uniform distribution. The value of the velocity was determined from the required Reynolds number.

In the electrochemical cell, the reaction of interest occurs at the cathode, as explained above. Thus, only one transport equation, that for the cation, is needed. The appropriate boundary condition for this ion at the cathode surface is C(cation) = 0 under current-limiting conditions. This condition implies that the electrochemical reaction rate at the cathode surface is much faster than the mass transport rate due to diffusion.

The second boundary condition states that the ion concentration approaches C(bulk) far from the cathode surface. Textbook treatments commonly set the asymptotic concentration at infinity to be the bulk concentration value, as is done for example in the treatment of the rotating disk electrode problem in the book by Newman [19]. In a computer simulation of a bounded structure we cannot quite make this assumption. Accordingly, we have set the concentration to be the bulk value at the mid-gap position. This constraint is set at a distance of 750 μ m from the surface. The chemical diffusion distance is approximately 5–10 μ m, as indicated in Figure 7, shown later. Hence, the results should be unaffected by the actual placement of this constraint; it is effectively at infinity.



Figure

Experimental arrangement used for electrochemical studies; that used for copper etching studies was similar.

The concentrations predicted by this model have validity only near the cathode. The concentration predicted near the anode surface does not account for the complex situation there, which should include the mass balance of the reacting ions, the oxidation of water at the high overpotential, and the resulting pH change. Other treatments of similar structures, such as the rotating disk structure, also do not describe the anode reaction in detail. We expect our treatment to be valid only within the wall jet region, where mixing of the anodic products into the cathode boundary layer is not expected.

With these assumptions, the equations of fluid motion are essentially uncoupled from the chemical equation. Thus, the flow problem can be separated from the chemical diffusion problem, and the simulation can be carried out in the following two steps:

- Calculating the steady-state flow pattern by numerically solving the Navier-Stokes fluid flow equations.
- 2. Using the computed flow pattern to calculate the distribution of the diffusing chemical species.

The mass transfer coefficient was calculated from the final finite element solution, which gives the concentration field throughout the fluid.

Experimental apparatus and procedures

Two experimental techniques were used to determine the mass transfer coefficients. In the first technique, a direct

measure of the mass transfer rate was obtained from an electrical current of a reaction under diffusion control. In the second, the mass transfer coefficients were calculated from an experimentally determined etching rate.

• Electrochemical probe

The electrochemical probe was part of an electrochemical cell that included reference and anode electrodes. A regulated power supply, an EG&G PARC Potentiostat/ Galvanostat Model 273, was used to apply a steady voltage between the cathode and the anode [16]. This potentiostat was controlled with an IBM industrial personal computer via a National Instruments general-purpose interface board.

The experimental arrangement used included the electrochemical cell, a centrifugal pump, three flow meters, and a holding tank, as shown in Figure 3. To control the flow rate, Y-pattern valves were used. One of the flowmeters consisted of a glass tube with a ball-type glass float and had a flow range of 0-5 liters per minute ($1/\min$); the second also consisted of a glass tube with a plummettype stainless steel float and had a flow range of 0.76–7.8 l/min; the third consisted of a thermoplastic rotameter with a plastic plummet float and had a flow range of 3.3-33 l/min. Use was made of an acrylic plastic tank measuring 30 cm by 30 cm by 33 cm. The actual total operating volume was 20 liters. The nozzle used for the experimentation had a 1.5-mm diameter. It was drilled in a 10-mm-thick block of polyvinyl chloride plastic. This block was attached to a cylindrical flow chamber to dampen flow pulsations from the centrifugal pump that was used.

Two different electrochemical probes were used in the present work. The first probe was a single microelectrode that was used to determine the mass transfer coefficients directly under the impinging jet. The second was an array of microelectrodes used to profile the mass transfer coefficients at a number of radii away from the nozzle axis.

The first probe consisted of a nickel wire 1.0 mm in diameter embedded in and electrically insulated from a planar electrode. The insulation thickness was 0.125 mm. The probe axis was located along the nozzle axis so that the stagnation point from the impinging jet was located at the center of the probe. This location permitted measurements of mass transfer directly underneath the jet. The large planar cathode electrode that surrounded the microelectrode was driven at the same voltage to provide an equipotential surface along the bottom of the flow channel. Then, readings from the microelectrode would represent measurements from a point in a planar reacting area. This larger electrode had dimensions of 101.6 mm by 31.8 mm. The 114.3 by 76.2-mm counter electrode, or anode, was positioned on the opposite side of the confinement channel and surrounded the nozzle. The area ratio of the anode with respect to the cathode was 2.4. This area was sufficient to ensure that the electrochemical

current was limited by diffusion at the cathode. The electrode arrangement used was that shown in Figure 2.

The second probe consisted of an array of microelectrodes made of 0.5-mm-diameter nickel wire. These wires were embedded in and electrically insulated from a larger electrode area. One microelectrode was aligned with the nozzle; the others were in pairs, symmetrically located along oppositely directed radii of 3.2, 7.7, 8.1, and 15.0 mm.

The gap between the cathode and anode was fixed at 1.5 mm, so that the ratio between nozzle diameter and gap was fixed at 1.0, a typical parameter used in wet-processing devices. The measurements were conducted at several flow rates to obtain Reynolds numbers based on nozzle diameter between 1400 and 13 000. The Schmidt number was approximately 2300.

The composition of the electrochemical solution was 2.0 N sodium hydroxide with 0.025 M potassium ferroand ferricyanide, all dissolved in de-aerated and de-ionized water. Some of the physical properties of the system used are summarized in **Table 1**.

To determine the electrical current passing through the microelectrodes and to the surrounding larger electrode, a set of operational amplifiers with selectable gain was used. These amplifiers acted as current followers with voltage output that was digitized with suitable analog-to-digital converters. The digitized signal was stored in memory and saved to magnetic disk. The signals obtained were filtered to eliminate experimental noise and then used to calculate the time-averaged Sherwood numbers.

• Controlled etching

The apparatus for the controlled etching experiments was similar to that shown in Figure 3. The nozzle was a drilled hole of length 12 mm and diameter 1.5 mm. The etching solution was recirculated by a centrifugal pump from a 5-liter holding tank through a valve, pressure gauge, feed chamber, and nozzle. The jet from the nozzle impinged on the surface of a 71- μ m-thick copper foil laminate. The foil was aligned with registration posts and formed one surface of a 1.5-mm rectangular channel. The nozzle velocity was determined from volumetric flow measurements and the nozzle diameter. Various experiments were performed at different Reynolds numbers (4300-7600) and lengths of time. The time-averaged local etch rate at radius r was calculated from the ratio of copper thickness etched divided by the time required to achieve that etching (T/t). The radius r was that of the resultant circular etch pattern. Some physical properties of the etching system are presented in **Table 2.** The value of $D_{\text{CuCl}_3}^{-2}$ and the surface saturation concentration for the calculation of $\Delta C_{\text{CuCl}}^{-2}$ were obtained from [23]. The value of saturation could thus be calculated from $C_{\text{sat}} \text{ (mol/m}^3\text{)} = 29.25 \times 10^{-6} [\text{Cl}^-]^2$, where [Cl⁻] is the concentration of free chloride ion.

Table 1 Some physical properties of the ferro-ferricyanide electrochemical system.

Cathode metal	Nickel (99.9% purity)
Cathode area, m ²	3.23×10^{-3}
Anode metal	Nickel (99.9% purity)
Anode area, m ²	7.74×10^{-3}
Supporting electrolyte	NaOH (2000 mol/m ³)
Concentration of ferricyanide ion, mol/m ³	25
Diffusion coefficient of ferricyanide ion, m ² /s	5.508×10^{-10}
Kinematic viscosity of solution, m²/s	1.2748×10^{-6}
Density of solution, kg/m ³	1085
Temperature, °C	25

Note: These properties were determined in this laboratory and cross-referenced with the literature [26].

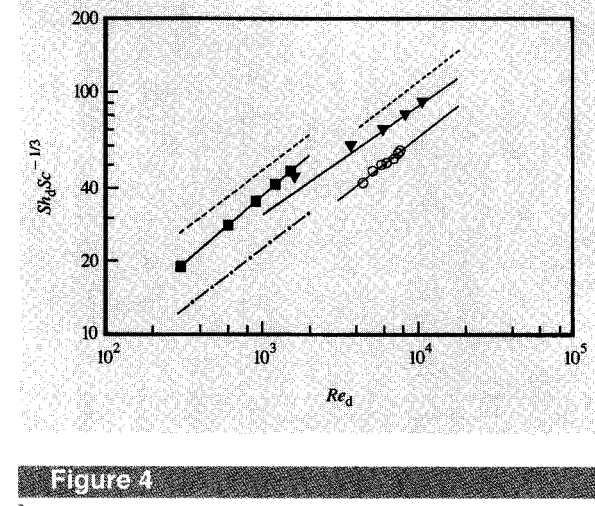
Table 2 Some physical properties of the etching system.

Density of copper metal, kg/m ³	8960
Molecular weight of copper	63.54
Saturation concentration of CuCl ₃ ⁻² , mol/m ³ [23]	220
Concentration of Cl ⁻ , mol/m ³	2700
Kinematic viscosity of solution, m ² /s	1.828×10^{-6}
Diffusion coefficient of active ion, m ² /s [23]	7.2×10^{-10}
Temperature, °C	25

The total Cl⁻ concentration was determined by titration with AgNO₃, and the viscosity was determined with a Cannon-Fenski viscosimeter.

Results and discussion

In the following we discuss data from the impingement zone and the wall jet region. A summary of Sherwood number data from the impingement zone is shown in Figure 4 for the electrochemical probe, controlled etching, and CFD work. Also shown in this figure, for comparison purposes, are the correlations obtained by Ching and Tsang [3] and Wang et al. [27] for impinging, unconfined, free jets. Figure 4 shows the mass transfer in dimensionless form vs. the Reynolds number of the flow. The Reynolds and Sherwood numbers in this figure are both based on nozzle diameter as their characteristic dimension. The data of Chin and Tsang are shown as two separate correlations, the two dashed lines, for the laminar and turbulent regions. The lower dashed-dotted line in Figure 4 is the correlation obtained by Wang et al. [27], as stated by Stevens and Webb [13] in their equation (8) for heat transfer from a single impinging free air jet. Table 3 summarizes the correlation coefficients.



Theoretical and experimental correlations at impingement region: CFD (\blacksquare), electrochemical probe (\blacktriangledown), etching (\bigcirc), Chin and Tsang [3] (laminar and turbulent region correlations) (---), and correlation obtained by Wang et al. [27] ($-\cdot\cdot-\cdot$).

Table 3 Summary of correlation coefficients for the impingement zone.

Reference	A	b (Reynolds number exponent)
CFD	0.742	0.56
Chin and Tsang [3] (laminar)	1.51	0.50
Chin and Tsang [3] (turbulent)	1.12	0.50
Electrochemical probe	1.35	0.45
Wang et al. [27]	0.717	0.50
Controlled etching	0.58	0.51

The results of the CFD model are plotted with square symbols in Figure 4. The calculations were limited to the laminar region, and to Reynolds numbers from 300 to 1500. The Sherwood number results were nearly proportional to the square root of the Reynolds number, a result predicted by the theoretical work of Watson [28]. The results are close to the electrochemical probe data given by the triangular symbols, and fall below the data for an unconfined jet of Chin and Tsang [3] (dashed line). Even with the laminar flow assumption, the prediction of the model is reasonable. These results form a starting point for more complete models that would include effects of turbulence.

The electrochemical probe results, shown in Figure 4 as the center data with the triangular symbols, are bracketed by the experimental correlations from the literature. The slope of the straight line is less steep than the work reported for unconfined jets, suggesting that the

confinement affects the mass transfer vs. Reynolds characteristic, making it less dependent on Reynolds number. Further characterization of this geometry would be required to determine the source of these differences.

The controlled etching results (circular symbols in Figure 4) show that the assumption of a mass-transfer-limited process for etching of an acidic cupric chloride solution is reasonable. The slope of the regression curve is similar to the values reported for unconfined jets by Chin and Tsang [3] and Wang et al. [27]. However, the values are smaller. This may have occurred because of the high concentrations of the reacting ions, the nonideality of the solution, and the assumed value of the diffusion coefficient. The electrochemical probe and the CFD results are based on dilute solution assumptions. Cupric chloride etching solutions are highly concentrated in order to obtain a high etching rate in practical applications, and are not expected to rigorously follow the predictions of models based on dilute solution theory [19].

The CFD model is useful for estimating etching rates for configurations being considered in the design of wet-process equipment. Associated experimental results are useful in the scaling of this work on a single confined jet to a large array of jets such as would be found in a manufacturing system.

In the wall jet region the fluid spreads laterally in a very thin sheet over the lower surface, as explained by Glauert [29]. The fluid slows down as it extends radially in the wall jet, and at a sufficiently large radius (in the transition region) actually stops and reverses direction near the work surface. This backflow is due to the formation of an eddy in which the wall jet lifts and starts to break up. This deceleration and eddy formation is a common occurrence in fluid motion, as described by Prandtl and Tietjens [30]. The cause of the deceleration is twofold: viscous shear forces due to the friction from the stationary surface, and a geometrical increase of the cross-sectional area of the fluid with increasing radius. Further out, the flow becomes laminar in the established flow region. Because the parallel plates have no predominant features to confine these eddies, they are slowly carried away by the flow. Timedependent simulations show that they convect outward from the jet, as is illustrated for example in Figure 5.

The lines shown in color depict separate streamlines of the flow at a number of time intervals immediately following the start-up of the flow. Such lines are contour lines of the stream function and are everywhere tangent to the fluid velocity [31]. For steady flows they are parallel to the path of a fluid particle. This is approximately true for the slowly changing flow depicted in the figure. The volume rate of flow is constant between any two streamlines. Hence, the flow speed in regions in which the streamlines are closely spaced, such as the wall jet region, is relatively rapid.

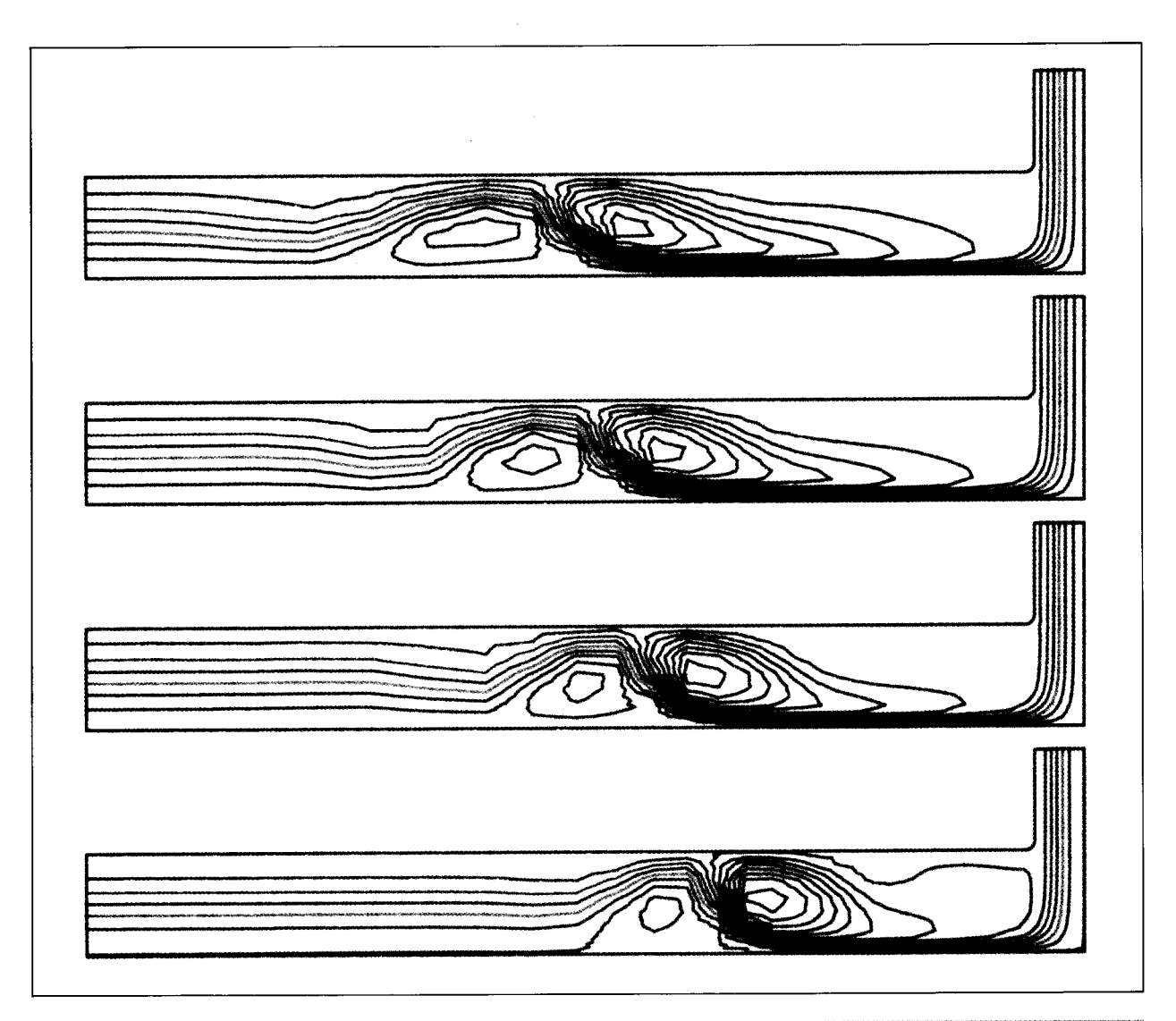
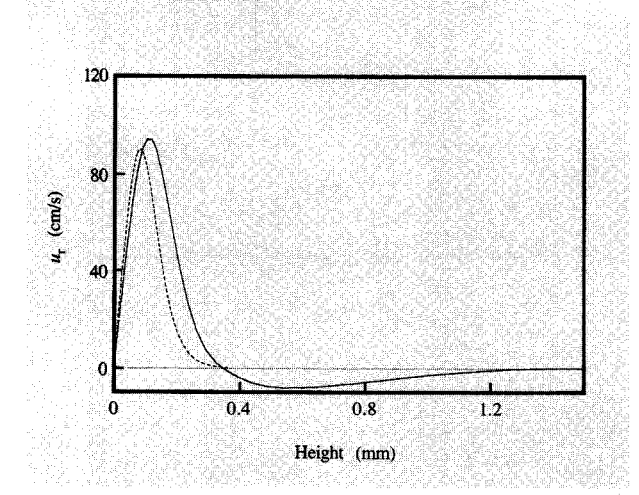


Figure 5

Illustrative fluid flow simulations, from CFD calculations. Flow patterns, progressing upward on the figure, are flow streamlines at successive times, showing convection of eddies. Total clapsed time is 250 milliseconds. The colored lines represent different streamlines.

For predicting etch rates near circuit features, a knowledge of the velocity profile adjacent to the feature is required. The velocity profile at a typical point in the wall jet region is shown in **Figure 6**. Also shown in this figure is the profile using Glauert's similarity solution for a free wall jet. Note the good agreement with both calculation methods. The differences that occur are due to the presence of recirculating eddies in the case of the confined jet. For a Reynolds number of 1500, **Figure 7** shows the thickness of the chemical boundary layer to be about $10~\mu m$. This is to be expected because of the smallness of the chemical diffusion coefficient (which is based on dilute solution theory).

Figure 8 shows the radial dependence of the Sherwood number as determined by the electrochemical probe and the controlled etching experiments. The characteristic distance used for calculating the Sherwood number Sh_r is the radial distance of Equation (2). The ordinate is the normalized Sherwood number, Sh_r/Sh_d . The abscissa, r/(d/2), is the radius normalized to the nozzle radius. When plotted in this manner, data at various Reynolds numbers can be combined in one plot. For example, the electrochemical probe data were taken at six Reynolds numbers between 1400 and 13 000; the controlled etching data were taken at seven Reynolds numbers between 4370 and 7570.





Calculated (via CFD) velocity profile across a channel (—). Radial distance was 3.175 mm. Glauert's similarity solution for a free wall jet [29] (---).

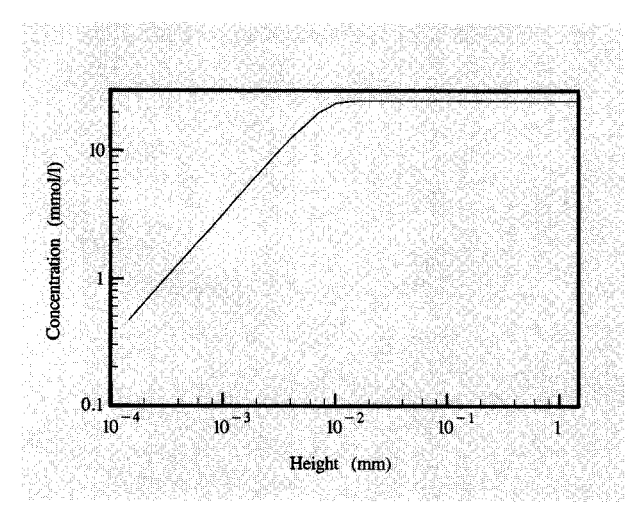
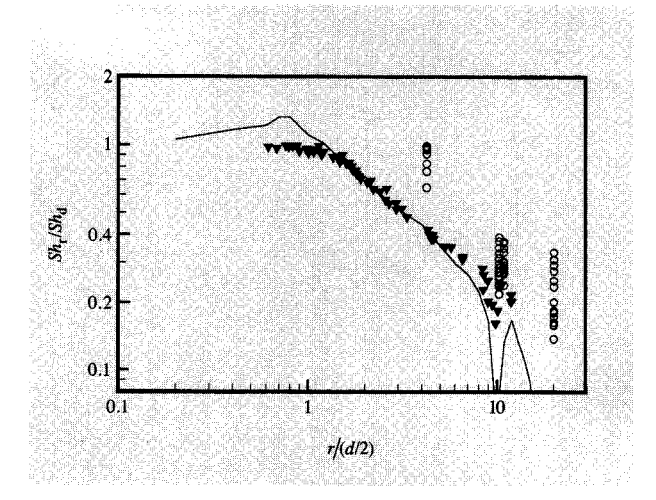


Figure 7

Calculated concentration profile across channel, at a radial distance of 3.175 mm. The electrochemical system is assumed to be operated under a limiting current condition, causing the ion concentration to be zero at the cathode surface.

Table 4 Slopes in the linear region of Figure 8.

Reference	Slope
Nakoryakov et al. [32] Electrochemical probe Controlled etching	-0.77 -0.87 -0.69



Floure 8

Normalized Sherwood number vs. normalized radius. Correlations obtained from Nakoryakov et al. [32] (-), from controlled etch data (\P) , and from electrochemical probe data (\circ) .

Three sets of data are shown in Figure 8: Nakoryakov's electrochemical data for free impinging jet [32] (solid curve), the electrochemical probe data (circles), and the controlled etching data (triangles) for a confined impinging jet. Nakoryakov's data show the relationship for a purely mass-transfer-limited process for a free impinging jet. The slopes in the linear region are given in **Table 4**.

The data from the electrochemical probe show a similar slope, with a radial shift. This may indicate that the boundary layer remains thin farther away than that for a free jet. For the controlled etching experiment, the slope was similar to the other two. The radial shift may have been absent because the etching experiment had a receding boundary layer which began at the edge of the etched circle in the foil. This effect was not present in the electrochemical probe because all of the areas internal to the circle are active, significantly changing the profile of the chemical boundary layer.

Figure 9 shows the dependence of the Sherwood number, Sh_r , on the Reynolds number, Re_r . Only experimental data in the radial asymptotic region are shown (regions W, T, and E of Figure 1). The solid line depicts the correlations of Alkire and Chen [4] and of Nakoryakov et al. [32] for a free impinging jet. The two sets of correlations are very similar and are shown as one line in this figure. Again we can see that the data from the electrochemical probe and the controlled etching experiment are of similar magnitude and have similar slopes. Both fall reasonably close to the correlations from the literature. The results again show that the copper

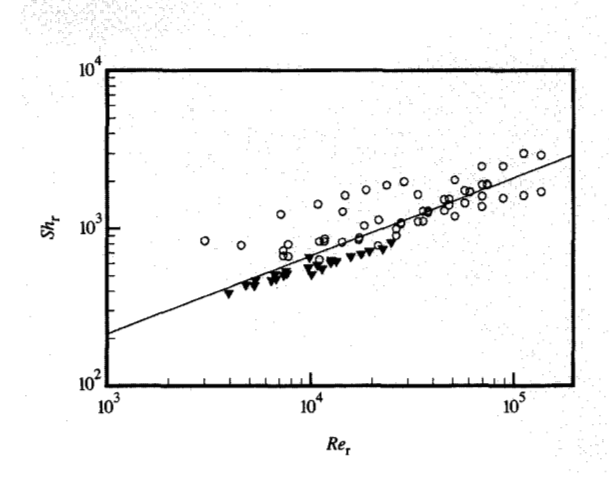


Figure 9

Sherwood number vs. Reynolds number, in the radial asymptotic region. Correlations obtained from Nakoryakov et al. [32] and from Alkire and Chen [4] (-), from controlled etch data (v), and from electrochemical probe data (o).

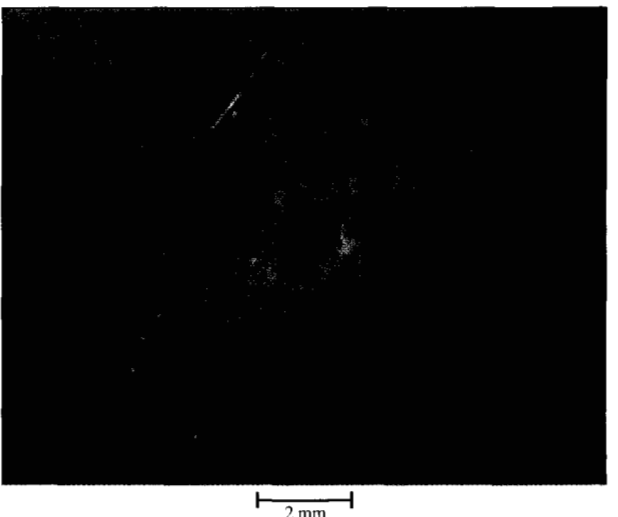
etching process may be considered as a mass-transferlimited process. Data shown in Figure 9 were taken at a variety of Reynolds numbers and radii.

An interesting observation was made on some of the etch patterns used in the controlled etching experiments. Right after breakthrough, when the radius of the etch figure was small, the etch pattern was not found to be circular. The etch pattern always had a distorted shape, which was quite often similar to two symmetrically facing quarter- or half-circular shapes. An illustration of the latter is shown in the lower portion of Figure 10. At larger etch radii, these circular shapes blended into a single larger circle. Landreth and Adrian [33] have reported the random wanderings of a submerged impinging jet. It is possible that our jets had a similar property that affected the shape of the etch pattern at small etch radii. The instability of the jet may have been caused by the shedding of eddies from either side of the nozzle. This is a property of many flows around objects. Also, any small tilt between the confinement plates or asymmetry of the flow resistance between the plates would break the axisymmetry of the flow, causing a complex shedding of eddies that might cause a slow side-to-side motion of the jet axis.

Concluding remarks

The combination of electrochemical studies, CFD simulation, and direct etch rate studies are useful methods for acquiring an understanding of the flow phenomena near an impinging jet. Our data show that copper etching with





Girinia III

Illustrative etch contours in copper foil located in the neighborhood of the stagnation point. Nozzle lengths used (upper and lower portions of the figure) were 12 and 9.5 mm, respectively.

acidic cupric chloride solutions can be approximated as a mass-transfer-limited process and that the etching follows established correlations from the literature. The results show that for purposes of scaling up an etching process, practical engineering data can be obtained using the approach described here. An extension of the approach to a system that uses arrays of fluid nozzles would be an appropriate next step.

Acknowledgments

The authors are indebted to the members of the support teams in the IBM Endicott facility, especially J. M. Parker, R. L. Burdick, E. M. Collins, L. J. Root, K. F. Conklin, L. C. Daniels, B. A. Kresge, and L. M. Croft.

They are also indebted to the following members of the development team, who have contributed in one way or another to the present effort: S. L. Bard, G. A. Bendz, M. J. Canestaro, N. P. Franchak, D. G. McBride, and R. J. Moore. Special thanks go to the reviewer of the paper for helpful suggestions.

FIDAP is a trademark of Fluid Dynamics International, Inc.

References

- 1. S. L. Bard, D. N. Christensen, J. J. Glenning, J. A. Nicoletti, and M. W. Urdanick, "Fluid Treatment Device," U.S. Patent 5,063,951, 1991.
- P. P. Pellegrino, "Apparatus for Electroplating, Deplating or Etching," U.S. Patent 4,174,261, 1979.
- D. T. Chin and C. H. Tsang, "Mass Transfer to an Impinging Jet Electrode," J. Electrochem. Soc. 125, 1461-1470 (1978)
- 4. R. C. Alkire and T. J. Chen, "High-Speed Selective Electroplating with Single Circular Jets," J. Electrochem. Soc. 129, 2424-2432 (1982).
- 5. G. K. Zin, "Fluid Applicator Apparatus," U.S. Patent 3,196,832, 1965.
- 6. T. A. Trabold and N. T. Obot, "Evaporation of Water with Single and Multiple Impinging Air Jets," J. Heat Transfer 113, 696-704 (1991).
- 7. D. E. Metzger, L. W. Florschuetz, D. I. Takeuchi, R. D. Behee, and R. A. Berry, "Heat Transfer Characteristics for Inline and Staggered Arrays of Circular Jets with Crossflow of Spent Air," J. Heat Transfer, Trans. ASME 101, 526 (1979).
- 8. L. W. Florschuetz, C. R. Truman, and D. E. Metzger, "Streamwise Flow and Heat Transfer Distributions for Jet Array Impingement with Crossflow," J. Heat Transfer, Trans. ASME 103, 337 (1981).
- 9. L. W. Florschuetz and H. H. Tseng, "Effect of Nonuniform Geometries on Flow Distributions and Heat Transfer Characteristics for Arrays of Impinging Jets," J. Eng. Gas Turbines Power, Trans. ASME 107, 68 (1985).
- 10. Papermaking and Paperboard Making, 2nd ed., R. G. MacDonald and J. N. Franklin, Eds., McGraw-Hill Book Co., Inc., New York, 1970, pp. 187ff.
- 11. H. Martin, "Heat and Mass Transfer Between Impinging Gas Jets and Solid Surfaces," Advanced Heat Transfer, Vol. 13, J. P. Harnett and T. F. Irvine, Eds., Academic Press, Inc., New York, 1977, p. 1.
- 12. X. Liu, V. J. H. Lienhard, and J. S. Lombara, "Convective Heat Transfer by Impingement of Circular Liquid Jets," *J. Heat Transfer* 113, 571-582 (1991).
- 13. J. Stevens and B. W. Webb, "Local Heat Transfer Coefficients Under an Axisymmetric, Single Phase Liquid Jet," J. Heat Transfer 113, 71-78 (1991).
- 14. S. Al-Sanea, "A Numerical Study of the Flow and Heat-Transfer Characteristics of an Impinging Laminar Slot-Jet Including Crossflow Effects," Int. J. Heat Mass Transfer 35, 2501 (1992).
- 15. R. B. Bird, W. E. Stewart, and E. N. Lightfoot, Transport Phenomena, John Wiley & Sons, Inc., New York, 1960,
- 16. L. P. Reiss and T. J. Hanratty, "Measurement of Instantaneous Rates of Mass Transfer to a Small Sink on a Wall," A.I.Ch.E. Journal 8, 245 (1962).
- 17. L. P. Reiss and T. J. Hanratty, "An Experimental Study of the Unsteady Nature of the Viscous Sublayer," A.I.Ch.E. Journal 9, 154 (1963).
- T. Mizushina, "The Electrochemical Method in Transport Phenomena," Advanced Heat Transfer, Vol. 7, J. P. Harnett and T. F. Irvine, Eds., Academic Press, Inc., New York, 1971, p. 87.

- 19. J. S. Newman, Electrochemical Systems, Prentice-Hall, Inc., Englewood Cliffs, NJ, 1973.
- D.-T. Chin and K.-L. Hsueh, "An Analysis Using the Chilton-Colburn Analogy for Mass Transfer to a Flat Surface from an Unsubmerged Impinging Jet,' Electrochim. Acta 31, 561 (1986).
- 21. A. P. Colburn, "A Method of Correlating Forced Convection Heat-Transfer Data and a Comparison with Fluid Friction," Trans. Amer. Inst. Chem. Eng. 29, 174
- 22. T. K. Sherwood, R. L. Pigford, and C. R. Wilke, Mass Transfer, McGraw-Hill Book Co., Inc., New York, 1975,
- 23. Maria Geo: Jou, "Anisotropic Chemical Etching of Copper in Acidic Cupric Chloride Solutions," Ph.D. thesis, University of Illinois at Urbana-Champaign, 1988.
- 24. FIDAP Theoretical Manual, Fluid Dynamics International, Inc., Evanston, IL, 1991.
- 25. G. K. Batchelor, An Introduction to Fluid Dynamics, Cambridge University Press, New York, 1967, p. 147.
- 26. J. R. Bourne, P. Dell'Ava, O. Dossenbach, and T. Post, "Densities, Viscosities, and Diffusivities in Aqueous Sodium Hydroxide-Potassium Ferri- and Ferrocyanide Solutions," J. Chem. Eng. Data 30, 160 (1985).
- 27. X. S. Wang, Z. Dagan, and L. M. Jiji, "Heat Transfer Between a Circular Free Impinging Jet and a Solid Surface with Non-uniform Wall Temperature or Wall Heat Flux-2. Solution for the Boundary Layer Region," Int. J. Heat Mass Transfer 32, 1361 (1989).
- 28. E. J. Watson, "The Radial Spread of a Liquid Jet over a
- Horizontal Plate," J. Fluid Mech. 20, 481 (1964). 29. M. B. Glauert, "The Wall Jet," J. Fluid Mech. 1, 625 (1956).
- 30. L. Prandtl and O. G. Tietjens, Applied Hydro- and Aeromechanics, Dover Publications, New York, 1934,
- 31. B. R. Munson, D. F. Young, and T. H. Okiishi, Fundamentals of Fluid Mechanics, John Wiley & Sons, Inc., New York, 1990, p. 330.
- 32. V. E. Nakoryakov, B. G. Pokusaev, and E. N. Troyan, "Impingement of an Axisymmetric Liquid Jet on a Barrier," Int. J. Heat Mass Transfer 21, 1175 (1978).
- 33. C. C. Landreth and R. J. Adrian, "Impingement of a Low Reynolds Number Turbulent Circular Jet onto a Flat Plate at Normal Incidence," Exp. Fluids 9, 74 (1990).

Received February 11, 1992; accepted for publication January 22, 1993

Oscar A. Moreno IBM Technology Products, 1701 North Street, Endicott, New York 13760 (MORENO at ENDVMTKL, oamoreno@vnet.ibm.com). Dr. Moreno is an Advisory Engineer in the Fluid Processes Department of the Technology Laboratory at the Endicott facility. He received the degree of Ingeniero Químico from the Universidad Autónoma de Puebla, México, in 1973, and M.S. and Ph.D. degrees in chemical engineering from the University of Illinois-Urbana in 1979 and 1983, respectively. From 1973 to 1976 he worked as a Process Engineer in Fertilizantes Fosfatados Mexicanos, Coatzacoalcos, Veracruz, México. He joined IBM at the Technology Laboratory in Endicott in 1983. His responsibilities have included the development of wet processes for the fabrication of computer packaging. He has used the electrochemical probe, heat transfer imaging, and laser doppler velocimetry to characterize fluid processes. He has also been involved in the scaling-up and automation of wet processes. Dr. Moreno is a member of the American Institute of Chemical Engineers and the Institute of Electrical and Electronics Engineers.

Robert H. Katyl IBM Technology Products, 1701 North Street, Endicott, New York 13760 (KATYL at ENDVMTKL). Dr. Katyl is a Senior Engineer in the Mechanical Analysis Department of the Technology Laboratory at the Endicott facility. He received S.B. and Ph.D. degrees in physics in 1964 and 1968 from the Massachusetts Institute of Technology. He worked at the Raytheon Corporation, Waltham, Massachusetts, in 1964 and 1966 on high-power microwave ferrite devices. He joined IBM in 1968 at the Technology Laboratory in Endicott, initially to work on applications of lasers and optics. He was an Adjunct Lecturer in Electrical Engineering at the State University of New York at Binghamton from 1986 to 1988. Dr. Katyl has recently been involved in the software simulation of problems involving electronic packaging and its manufacture. His current interests include fluid flow and solder meniscus modeling. Dr. Katyl has received four IBM Invention Achievement Awards. He is a member of the Institute of Electrical and Electronics Engineers.

Jeffrey D. Jones IBM Technology Products, 1701 North Street, Endicott, New York 13760 (JJONES at ENDVM1, jjones@endvm1.vnet.ibm.com). Mr. Jones joined IBM in 1988 as a Manufacturing Engineer in circuit panel manufacturing. He received a B.S. degree in chemical engineering from Brigham Young University in 1987. He is currently involved in the development and application of impinging jet devices for panel manufacturing.

Peter A. Moschak IBM Technology Products, 1701 North Street, Endicott, New York 13760 (MOSCHAK at ENDVMTKL). Mr. Moschak is a Technical Laboratory Specialist in the Technology Laboratory at the Endicott facility. He joined IBM in 1977 to work in the Metal Plating Department at that facility. From 1979 to 1985 he worked in the Advanced Circuit Packaging Laboratory as a Process Technician and a Manufacturing Methods Specialist. He is currently working on the development of wet processing for plating and etching. Mr. Moschak's interests include the characterization of fluid processing devices using laser doppler velocimetry and electrochemical and heat transfer techniques. Also, he is involved in the automation and optimization of plating and etching processes. He holds a U.S. patent on an advanced polymer composite.

